Electronic Supplementary Information

Formation of Fe(III)-As(V) complexes: effect on the solubility of ferric hydroxide precipitates and molecular structural identification

Qiantao Shi[a], George E. Sterbinsky[b], Shujuan Zhang[a], Christos Christodoulatos[a], George P. Korfiatis[a], and Xiaoguang Meng[a]*

[a]Center for Environmental Systems, Stevens Institute of Technology, Hoboken, New Jersey 07030, United States

[b]Advanced Photon Source, Argonne National Laboratory, Argonne, Illinois - 60439, United States

Tel: 001 201-216-8014; Fax: 001 201-216-8303

E-mail: xmeng@stevens.edu

Number of Pages: 15

Number of Figures: 7

Number of Tables: 5

Particle size analysis by dynamic light scattering

The hydrodynamic diameter (d) was calculated from the Stokes–Einstein equation assuming spherical particles:

$$d = \frac{k_B T}{3\pi\eta D} \quad (1)$$

where k_B is the Boltzmann's constant, T is the absolute temperature, D is the diffusion coefficient, and η is the viscosity of the water in this study. Particle size distributions and Poly Dispersity Index (PDI) were obtained from the intensity autocorrelation function by the cumulant and CONTIN methods, respectively, using the Malvern software (DTS Version 5.00).

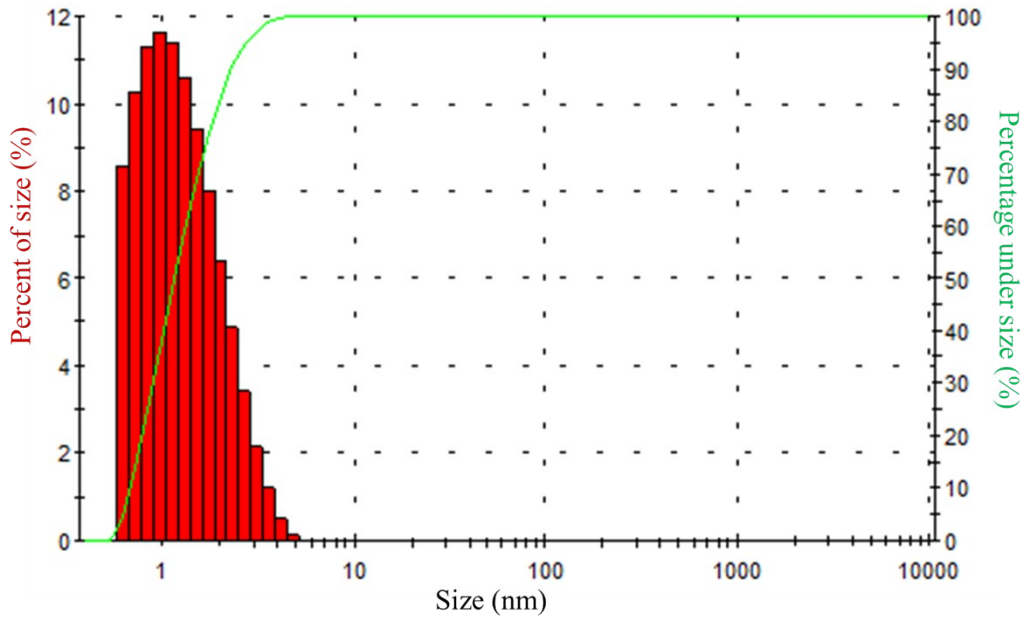

Figure S1. Size distribution of the filtered 100 mM $FeCl_3$ and As(V) solution after 180 days mixing.

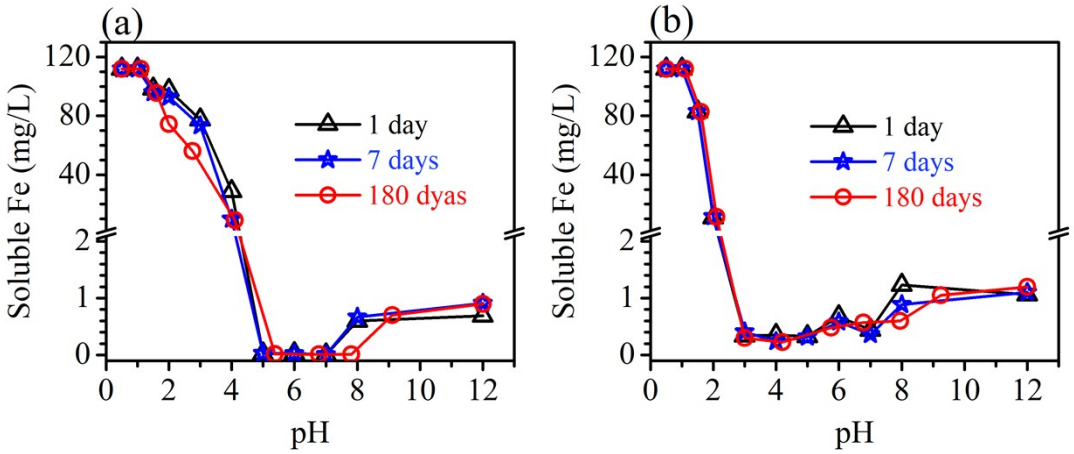

Figure S2. Soluble Fe concentrations in 2 mM Fe(III) solutions without (a) and with (b) 2 mM As(V) after 1 (black triangles), 7 (blue stars), and 180 (red circles) days mixing as a function of pH (ionic strength = 0.01 M NaCl, room temperature)

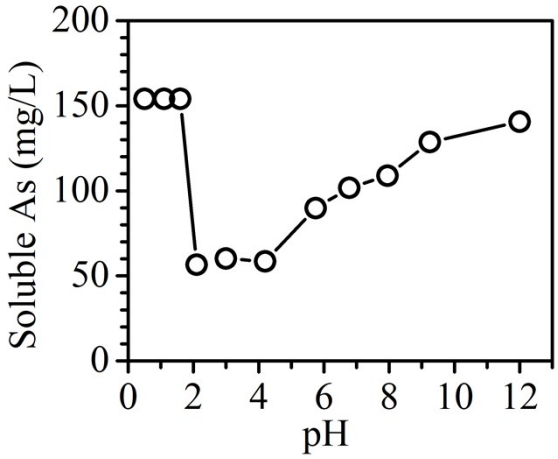

Figure S3. Soluble As concentrations in 2 mM Fe(III) solutions in the presence of 2 mM As(V) after 180 days mixing as a function of pH (ionic strength = 0.01 M NaCl, room temperature)

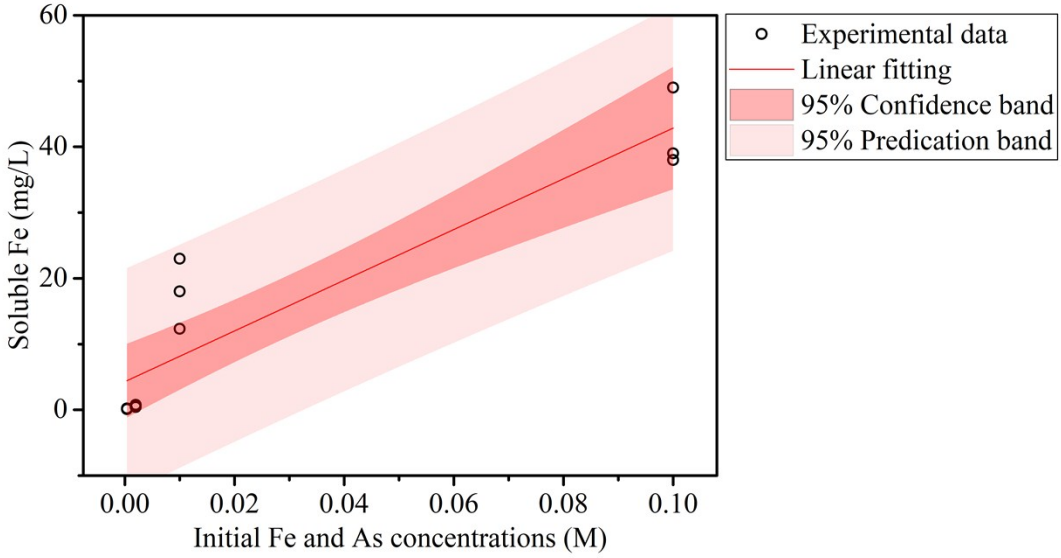

Figure S4. Linear fitting of the soluble Fe against the initial Fe and As concentrations.

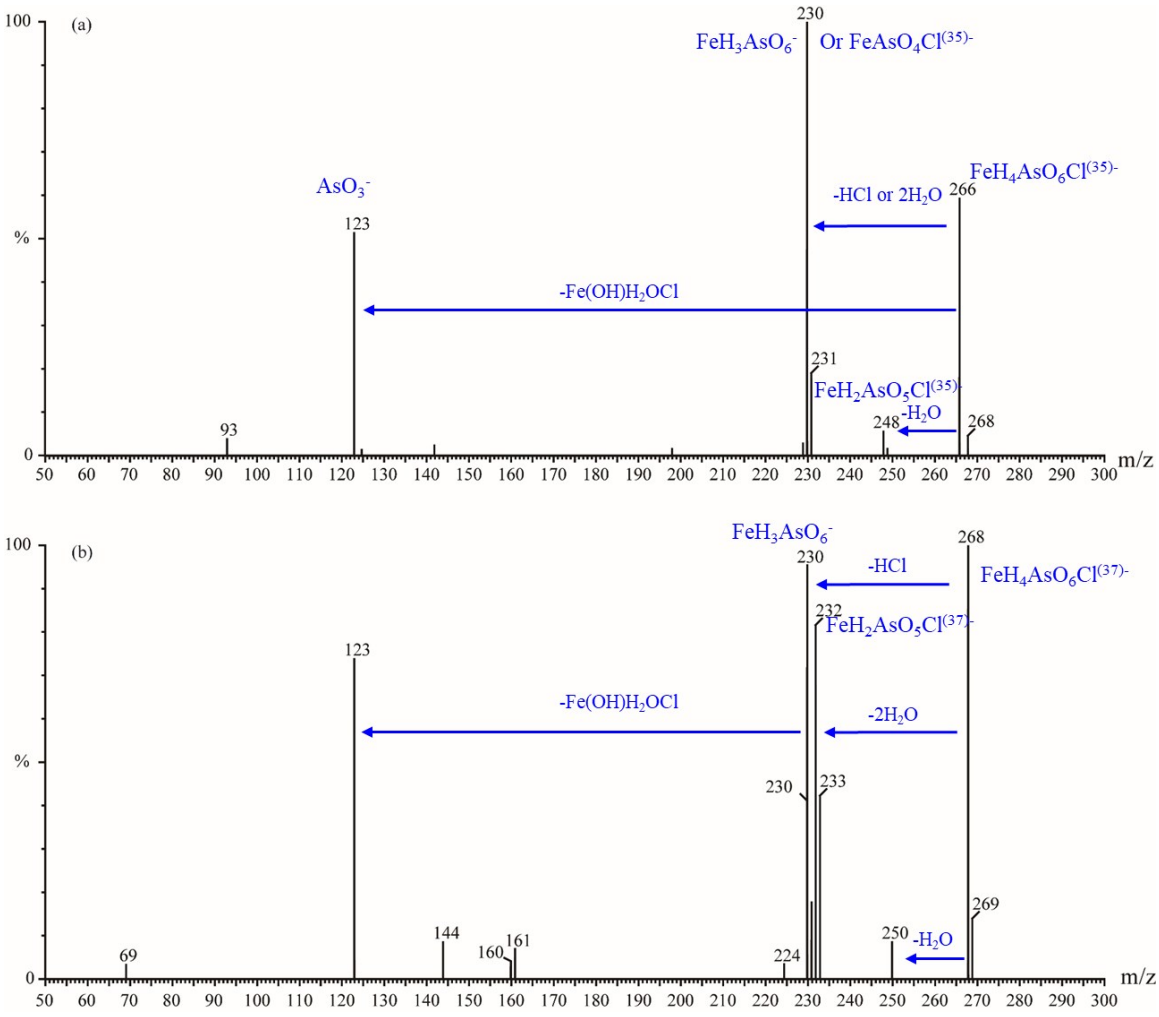

Figure S5. ESI-MS/MS analyses of daughter ions for peaks at m/z 266 (a) and 268 (b).

ATR-FTIR analysis

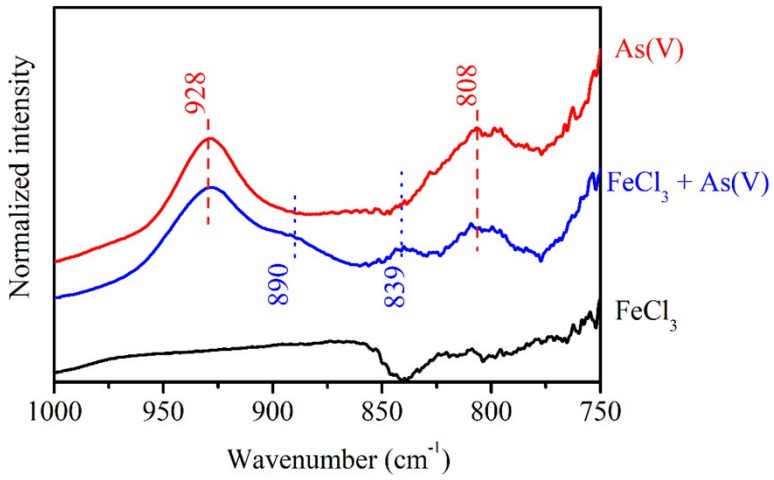

Figure S6. ATR-FTIR spectra of $FeCl_3$ solutions without (black) and with (blue) As(V), and As(V) solution at pH = 0.5 (Fe concentration = 10 mM, As concentration = 10 mM, HCl = 4%).

EXAFS data analysis

EXAFS data analysis was performed using the ATHENA and ARTEMIS programs in the Demeter computer package[1, 2]. The analysis procedure was similar to our previous studies [3, 4]. The raw data were averaged and normalized. The EXAFS signal $\chi(k)$ was extracted from the measured data using the AUTOBK algorithm[5] where k is the photoelectron wave number. The primary quantity for EXAFS is then $\chi(k)$, the oscillations as a function of photoelectron wave number. $\chi(k)$ was weighted by k^3 to account for the dampening of oscillations with increasing k. The different frequencies in the oscillations in χ(k) correspond to different near-neighbor coordination shells, which can be described and modeled according to the EXAFS equation[6-9]:

$$\chi(k) = \sum_j \frac{N_j f_j(k) e^{-2k^2\sigma_j^2}}{kR_j^2} \sin[2kR_j + \delta_j(k)]$$

where f(k) and $\delta(k)$ represent the photoelectron backscattering amplitude and phase shift, respectively, N is the number of neighboring atoms, R is the distance to the neighboring atom, and σ^2 is the Debye-Waller factor representing the disorder in the neighbor distance. The k^3 weighted EXAFS spectrum in k-space (Å^{-1}) was Fourier transformed (FT) in R-space (Å). K range from 2 to 12 Å^{-1} was selected for As K-edge EXAFS fitting, while K range from 2 to 10 or 11 Å^{-1} was selected for Fe K-edge EXAFS fitting. The experimental spectra were fitted with single-scattering theoretical phase-shift and amplitude functions calculated with the *ab initio* computer code FEFF6[10] using atomic clusters generated from the crystal structure of scorodite[11]. The values of many-body amplitude reduction factor (S_0^2) were established as 0.93~0.98 by fixing the coordination number (4) of As-O shell for As K-edge. On the other hand, the S_0^2 values for Fe K-edge was estimated as 0.95 by reasonable CN of Fe-O shell (4~6) and Fe-Cl shell (0~1). The parameters such as interatomic distance (R), coordination number (CN), the difference in threshold energy (ΔE_0) and Debye-Waller factor (σ^2) were first established with reasonable guesses and

then fitted in R-space. The error in the overall fits was determined using the R-factor, the goodness-of-fit parameter: R-factor = $\Sigma(\chi_{data} - \chi_{fit})^2/\Sigma(\chi_{data})^2$. Good fits occur for R-factor < 0.05.

Table S1. Structure parameters derived from As K-edge EXAFS analysis.

Solutions	Path	CN [a]	R (Å) [b]	σ^2 (Å^2) [c]	ΔE_0 (eV) [d]	R-factor [e]
As(V)	As-O	4[f]	1.70(1)	0.002(1)	7.5	0.017
As(V) + Fe(III)	As-O	4[f]	1.70(1)	0.002(1)	7.5	0.018
	As-Fe	0.7(2)	3.05(5)	0.003(1)		

[a]coordination number. [b]interatomic distance. [c]Debye-Waller factor. [d]threshold energy shift. [e]goodness-of-fit parameter: R-factor = $\Sigma(\chi_{data} - \chi_{fit})^2/\Sigma(\chi_{data})^2$. [f]parameter was fixed in the fitting process. Parentheses: the estimated parameter uncertainties are listed in parentheses, representing the errors in the last digit; values without reported errors were fixed during fitting.

Table S2. Structure parameters derived from Fe K-edge EXAFS analysis.

Solutions	Path	CN [a]	R (Å) [b]	σ^2 (Å^2) [c]	ΔE_0 (eV) [d]	R-factor [e]
Fe(III)	Fe-O	5.2(4)	2.03(1)	0.006(1)	6.2	0.004
	Fe-Cl	0.3(1)	2.32(2)	0.008(3)		
	Fe-Fe	3.8(7)	3.64(6)	0.027(5)		
Fe(III) + As(V) in 4% HCl	Fe-O	4.9(7)	1.99(1)	0.002(1)	-4.1	0.019
	Fe-Cl	0.2(1)	2.31(3)	0.007(2)		
	Fe-As	0.8(1)	3.12(4)	0.003(1)		
	Fe-Fe	0.3(1)	3.54(14)	0.017(6)		
Fe(III) + As(V) at pH 7 (filtered)	Fe-O	5.1(8)	1.98(1)	0.009(2)	-3.2	0.023
	Fe-Cl	0.4(2)	2.33(3)	0.008(3)		
	Fe-As	2.3(7)	3.18(1)	0.006(3)		

[a]coordination number. [b]interatomic distance. [c]Debye-Waller factor. [d]threshold energy shift. [e]goodness-of-fit parameter: R-factor = $\Sigma(\chi_{data} - \chi_{fit})^2/\Sigma(\chi_{data})^2$. Parentheses: the estimated parameter uncertainties are listed in parentheses, representing the errors in the last digit; values without reported errors were fixed during fitting.

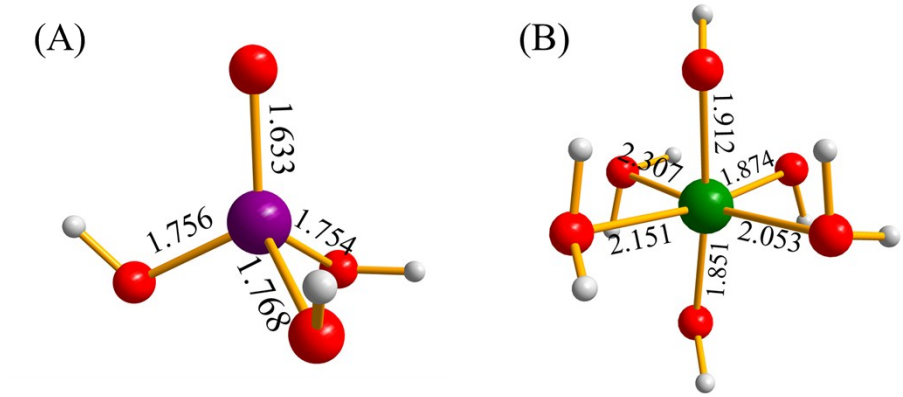

Figure S7. DFT calculated molecules of H_3AsO_4 (A) and $Fe(OH)_3(OH_2)_3$ (B). Atoms: purple = As, red = O, gray = H, green = Fe. Bond lengths of As-O and Fe-O are labeled in the figure with the unit of angstrom (Å).

Table S3. Total energies of Fe(III), As(V), and possible Fe(III)-As(V) complexes.

Description	Species	Clusters	*E* (eV)
Reactants	H_3AsO_4	H_3AsO_4	-112.024
	FeO_6	$Fe(OH)_3(OH_2)_3$	-197.181
	Water molecule	H_2O	-31.001
	HCl	HCl	-21.614
Single As with **bidentate**	FeH_8AsO_8	$(OH_2)_2(OH)_2FeO_2As(OH)_2$ Figure 5-A0	-247.499
		$(OH_2)_2(OH)_2FeO_2HAsO_2H$ Figure 5-A1	-245.924
		$(OH_2)_2(OH)_2Fe(OH)_2AsO_2$ Figure 5-A2	-245.616
	FeH_7AsO_7Cl	$(OH_2)_2(OH)ClFeO_2As(OH)_2$ Figure 5-B0	-238.699
		$(OH_2)_2(OH)ClFeO_2HAsO_2H$ Figure 5-B1	-237.709
		$(OH_2)_2(OH)ClFe(OH)_2AsO_2$ Figure 5-B2	-238.775
Single As with **monodentate**	FeH_9AsO_8Cl	$(OH_2)_3(OH)ClFeOAs(OH)_3$ Figure 5-C	-270.554
Double As with **bidentate**	$FeH_7As_2O_{10}$	$(OH_2)OHFe((OH)_2AsO_2)_2$ Figure 6-A	-296.929
	$FeH_6As_2O_9Cl$	$(OH_2)ClFe((OH)_2AsO_2)_2$ Figure 6-C	-287.769
Double As with **monodentate**	$FeH_{11}As_2O_{12}$	$(OH_2)_3OHFe((OAsO(OH)_2)_2$ Figure 6-B	-360.790
	$FeH_{10}As_2O_{11}Cl$	$(OH_2)_3ClFe((OAsO(OH)_2)_2$ Figure 6-D	-352.106

Table S4. Calculated binding energies ($E_{binding}$ (kJ/mol)) of possible Fe(III)-As(V) complexes.

Complexes	Reactions	*BE* (kJ/mol)
$(OH_2)_2(OH)_2FeO_2As(OH)_2$ Figure 5-A0	$Fe(OH)_3(OH_2)_3 + H_3AsO_4 \rightarrow (OH_2)_2(OH)_2FeO_2As(OH)_2 + 2H_2O$	-28.651
$(OH_2)_2(OH)_2FeO_2HAsO_2H$ Figure 5-A1	$Fe(OH)_3(OH_2)_3 + H_3AsO_4 \rightarrow (OH_2)_2(OH)_2FeO_2HAsO_2H + 2H_2O$	123.309
$(OH_2)_2(OH)_2Fe(OH)_2AsO_2$ Figure 5-A2	$Fe(OH)_3(OH_2)_3 + H_3AsO_4 \rightarrow (OH_2)_2(OH)_2Fe(OH)_2AsO_2 + 2H_2O$	153.067
$(OH_2)_2(OH)ClFeO_2As(OH)_2$ Figure 5-B0	$Fe(OH)_3(OH_2)_3 + H_3AsO_4 + HCl \rightarrow (OH_2)_2(OH)ClFeO_2As(OH)_2 + 3H_2O$	-85.244
$(OH_2)_2(OH)ClFeO_2HAsO_2H$ Figure 5-B1	$Fe(OH)_3(OH_2)_3 + H_3AsO_4 + HCl \rightarrow (OH_2)_2(OH)ClFeO_2HAsO_2H + 3H_2O$	10.232
$(OH_2)_2(OH)ClFe(OH)_2AsO_2$ Figure 5-B2	$Fe(OH)_3(OH_2)_3 + H_3AsO_4 + HCl \rightarrow (OH_2)_2(OH)ClFe(OH)_2AsO_2 + 3H_2O$	-92.647
$(OH_2)_3(OH)ClFeOAs(OH)_3$ Figure 5-C	$Fe(OH)_3(OH_2)_3 + H_3AsO_4 + HCl \rightarrow (OH_2)_3(OH)ClFeOAs(OH)_3 + 2H_2O$	-167.656
$(OH_2)OHFe((OH)_2AsO_2)_2$ Figure 6-A	$Fe(OH)_3(OH_2)_3 + 2*H_3AsO_4 \rightarrow (OH_2)OHFe((OH)_2AsO_2)_2 + 4H_2O$	28.417
$(OH_2)_3OHFe((OAsO(OH)_2)_2$ Figure 6-B	$Fe(OH)_3(OH_2)_3 + 2*H_3AsO_4 \rightarrow (OH_2)_3OHFe((OAsO(OH)_2)_2 + 2H_2O$	-150.931
$(OH_2)ClFe((OH)_2AsO_2)_2$ Figure 6-C	$Fe(OH)_3(OH_2)_3 + 2*H_3AsO_4 + HCl \rightarrow (OH_2)ClFe((OH)_2AsO_2)_2 + 5H_2O$	6.510
$(OH_2)_3ClFe((OAsO(OH)_2)_2$ Figure 6-D	$Fe(OH)_3(OH_2)_3 + 2*H_3AsO_4 + HCl \rightarrow (OH_2)_3ClFe((OAsO(OH)_2)_2 + 3H_2O$	-218.721

Table S5. Estimated equilibrium constants (Log K) of soluble As(V)-Fe(III)-As(V) complex at pH 7.

Initial Fe (M)	Initial As (M)	Initial Cl (M)	Log K
0.0004	0.0004	0.01	6.45
0.002	0.002	0.01	5.10
0.01	0.01	0.01	4.50
0.1	0.1	0.01	1.86

The equilibrium constants were derived from the following equation (S1) based on our spectroscopic measurements and DFT calculations:

$$Log\ K = Log\ \frac{[As - Fe(Cl) - As]}{[Fe] * [As]^2 * [Cl]} \quad \text{(S1)}$$

While the concentration of [As-Fe(Cl)-As] is the measured Fe concentration at pH 7 after filtration using a 0.02 μm pore size filter.

References:

(1) Newville, M., IFEFFIT: interactive XAFS analysis and FEFF fitting. *J. Synchrotron Radiat.* **2001,** *8*, 322-324.
(2) Ravel, B.; Newville, M., ATHENA, ARTEMIS, HEPHAESTUS: data analysis for X-ray absorption spectroscopy using IFEFFIT. *J. Synchrotron Radiat.* **2005,** *12*, 537-541.
(3) Shi, Q. T.; Yan, L.; Chan, T. S.; Jing, C. Y., Arsenic Adsorption on Lanthanum-Impregnated Activated Alumina: Spectroscopic and DFT Study. *ACS Appl. Mat. Interfaces* **2015,** *7*, 26735-26741.
(4) Peng, X.; Xi, B.; Zhao, Y.; Shi, Q.; Meng, X.; Mao, X.; Jiang, Y.; Ma, Z.; Tan, W.; Liu, H.; Gong, B., Effect of Arsenic on the Formation and Adsorption Property of Ferric Hydroxide Precipitates in ZVI Treatment. *Environ. Sci. Technol.* **2017,** *51*, 10100-10108.
(5) Newville, M.; Livins, P.; Yacoby, Y.; Rehr, J. J.; Stern, E. A., Near-Edge X-Ray-Absorption Fine-Structure of Pb - a Comparison of Theory and Experiment. *Phys. Rev. B* **1993,** *47*, 14126-14131.
(6) Stern, E. A.; Sayers, D. E.; Lytle, F. W., Extended x-ray-absorption fine-structure technique. III. Determination of physical parameters. *Phys. Rev. B* **1975,** *11*, 4836-4846.
(7) Lytle, F. W.; Sayers, D. E.; Stern, E. A., Extended x-ray-absorption fine-structure technique. II. Experimental practice and selected results. *Phys. Rev. B* **1975,** *11*, 4825-4835.
(8) Stern, E. A., Theory of the extended x-ray-absorption fine structure. *Phys. Rev. B* **1974,** *10*, 3027-3037.
(9) Sayers, D. E.; Stern, E. A.; Lytle, F. W., New Technique for Investigating Noncrystalline Structures: Fourier Analysis of the Extended X-Ray---Absorption Fine Structure. *Phys. Rev. Lett.* **1971,** *27*, 1204-1207.
(10) Deleon, J. M.; Rehr, J. J.; Zabinsky, S. I.; Albers, R. C., Abinitio Curved-Wave X-Ray-Absorption Fine-Structure. *Phys. Rev. B* **1991,** *44*, 4146-4156.
(11) Kitahama, K.; Kiriyama, R.; Baba, Y., Refinement of Crystal-structure of Scorodite. *Acta Crystallogr. Sect. B-Struct. Sci.* **1975,** *31*, 322-324.